Identification of genetic drivers of plasma lipoprotein size in the Diversity Outbred mouse population

Tara R. Price[1], **Christopher H. Emfinger**[1], **Kathryn L. Schueler**[1], **Sarah King**[2], **Rebekah Nicholson**[3], **Tim Beck**[4], **Brian S. Yandell**[5], **Scott A. Summers**[3], **William L. Holland**[3], **Ronald M. Krauss**[2], **Mark P. Keller**[1], **and Alan D. Attie**[1]*

[1]Department of Biochemistry, University of Wisconsin–Madison, Madison, WI, USA; [2]School of Medicine, University of California–San Francisco, San Francisco, CA, USA; [3]Department of Nutrition and Integrative Physiology, University of Utah, Salt Lake City, UT, USA; [4]Department of Genetics and Genome Biology, University of Leicester, Leicester, UK; and [5]Department of Statistics, University of Wisconsin–Madison, Madison, WI, USA

Abstract Despite great progress in understanding lipoprotein physiology, there is still much to be learned about the genetic drivers of lipoprotein abundance, composition, and function. We used ion mobility spectrometry to survey 16 plasma lipoprotein subfractions in 500 Diversity Outbred mice maintained on a Western-style diet. We identified 21 quantitative trait loci (QTL) affecting lipoprotein abundance. To refine the QTL and link them to disease risk in humans, we asked if the human homologs of genes located at each QTL were associated with lipid traits in human genome-wide association studies. Integration of mouse QTL with human genome-wide association studies yielded candidate gene drivers for 18 of the 21 QTL. This approach enabled us to nominate the gene encoding the neutral ceramidase, *Asah2*, as a novel candidate driver at a QTL on chromosome 19 for large HDL particles (HDL-2b). To experimentally validate *Asah2*, we surveyed lipoproteins in *Asah2*$^{-/-}$ mice. Compared to wild-type mice, female *Asah2*$^{-/-}$ mice showed an increase in several lipoproteins, including HDL. Our results provide insights into the genetic regulation of circulating lipoproteins, as well as mechanisms by which lipoprotein subfractions may affect cardiovascular disease risk in humans.

Supplementary key words lipoproteins/metabolism • genomics • apolipoproteins • HDL • LDL • VLDL • ceramides • genetic architecture

High concentrations of LDL-C are associated with increased CVD risk. Interventions to reduce LDL-C result in improved cardiovascular outcomes. Small dense LDL particles are associated with CVD, including coronary artery disease and stroke (1), and are strong predictors of cardiovascular events (2). Likewise, larger HDL-2b particles are better predictors of coronary heart disease than small, dense HDL-3, LDL-C, or HDL-C levels (3–5). Variation in protein and lipid composition and particle size can affect lipoprotein function (6–9).

Genetically diverse mouse populations, resulting from intercrossing or outcrossing inbred strains, can be used to discover the genetic drivers of lipoprotein abundance and composition. For example, intercross mouse populations identified gene loci affecting apolipoprotein (Apo) A2 (10). In an intercross study involving the RIIIS/J and 129S1/SvImJ mouse strains, eight unique loci affecting plasma cholesterol and causative genes within the loci were identified (11). Panels of recombinant inbred mouse strains have been used to leverage naturally occurring polymorphisms, which showed heterogeneity in lipoprotein size and apolipoprotein composition (12). The hybrid mouse diversity panel, a collection of 100 mouse strains, utilizes natural strain variation in a systems genetics approach to identify genetic drivers of phenotypes (13). A meta-analysis of nearly 5000 hybrid mouse diversity panel mice identified 26 significant loci associated with HDL-C. Several loci, including one for ApoA2, were consistent with previous reports, whereas other loci provided novel insights into gene-environment interactions (14).

The use of outcrossed mouse populations, including the collaborative cross (CC), brings additional genetic diversity to mouse genetic screens. In a study using 25 CC strains, increased adiposity and liver steatosis were associated with increasing total, HDL, and LDL cholesterol (15). Key genetic regulators of hepatic lipids were linked to diet-induced changes in liver steatosis severity and plasma lipid measures. Leveraging the genetic diversity of the diversity outbred (DO) mouse population, an outbred stock derived from eight founder strains of the CC, three loci were identified for plasma cholesterol (16).

*For correspondence: Alan D. Attie, adattie@wisc.edu.

https://doi.org/10.1016/j.jlr.2023.100471

In the present study, we utilized the DO mouse population to determine quantitative lipoprotein subclasses, identify quantitative trait loci (QTL) for several subclasses, and nominate candidate genetic drivers of lipoprotein particle sizes. We identified several known cholesterol-related genes, *Apoa2* and *Foxo1*, as well as novel loci associated with plasma cholesterol.

MATERIALS AND METHODS

Animal husbandry—founder and DO mice

All animal protocols were approved by the Animal Care and Use Committee at the University of Wisconsin-Madison. The eight founder strains (C57BL/6J [B6]; A/J; 129S1/SvImJ [129]; NOD/ShiLtJ [NOD]; NZO/HILtJ [NZO]; PWK/PhJ [PWK]; WSB/EiJ [WSB]; and CAST/EiJ [CAST]) and DO mice were purchased from Jackson Laboratories (Bar Harbor, ME) and maintained at the University of Wisconsin-Madison, as previously described (17, 18). Briefly, founder mouse strains were fed standard laboratory chow (Formulab Diet 5008; LabDiets, Brentwood, MO) or given a high-fat, high-sucrose diet (HFHS; TD.08811; Envigo, Madison, WI) for 18 weeks. DO mice were maintained on the same HFHS diet as the founder mice for 16 weeks. Animals were euthanized at 22 weeks of age, and plasma was collected and stored at −80°C.

Animal husbandry—*Asah2* mice

Asah2 mice were generated by Richard Proia (National Institutes of Health [NIH]) (19) and provided to the Summers/Holland laboratory. All animal procedures were performed in compliance with the protocols approved by the Institutional Animal Care and Use Committee at the University of Utah and adhered to NIH standards. Male (n = 5–6 per genotype) and female (n = 4–7 per genotype) mice were maintained under standard laboratory conditions at a temperature of 22–24°C, in groups of 2–5 mice, with a 12 h light/dark cycle. Mice were allowed ad libitum access to food and water unless fasting conditions were required for experimental procedures. Animals were fed a normal chow diet from the age of 4 weeks and transitioned to an HFD (60% total energy; D12492; Research Diets, Inc, New Brunswick, NJ) at 9 weeks of age for 16 weeks. At 25 weeks of age, mice were anesthetized with isoflurane, and blood collected by cutting the brachial artery. Whole blood was collected into vacutainers coated with 20% K_2EDTA, centrifuged at 7,500 g for 7.5 min, and plasma was separated. Plasma was stored at −80°C.

Plasma lipoprotein fractionation by ion mobility analysis

To analyze lipoprotein class size, plasma lipoproteins were separated by ion mobility analysis as previously described (20, 21). Briefly, lipoproteins were harvested on paramagnetic particles, washed to remove free salt and proteins (e.g., IgG, albumin, and transferrin), and then resuspended in 25 mM ammonium acetate. Lipoproteins were then fractionated and quantified by summing the total number of particles within specific size ranges. Supplemental Table S1 shows the lipoprotein subclasses, their size ranges, and nomenclature.

QTL mapping of plasma lipoprotein phenotypes

Mapping of plasma lipoproteins for QTL analysis was performed as previously described (17). Briefly, 478 DO mice (236 females and 242 males) were obtained from Jackson Laboratories (Bar Harbor, ME) and maintained on a HFHS diet (TD.08811; Envigo) for 16 weeks, and plasma was collected for lipoprotein sizing by ion mobility analysis. Lipoprotein phenotype data were rankZ-transformed to achieve a normal distribution prior to mapping. Genetic mapping was performed using the R/qtl2 package with kinship correction to identify QTL using the GRCm38 genome build and Ensembl 75 for gene annotation. Genome scans used sex, mouse cohort (wave), and technical batch as additive covariates. As previously described, logarithm of odds (LOD) thresholds were defined through permutation testing to establish a genome-wide family wide error rate for genome-wide QTL (22, 23). A LOD greater than 6.0 was used as the threshold for identifying suggestive QTL, and a LOD greater than 7.4 identified significant QTL.

Identification of candidate causal genes

To identify candidate causal genes, we explored single nucleotide polymorphisms (SNPs) at each mouse locus, significant associations in human genome-wide association studies (GWAS) to cardiometabolic traits, and phenotyping data available from the International Mouse Phenotyping Consortium (IMPC; mousephenotype.org), as well as incorporating known lipoprotein biology from the published literature. We first surveyed the SNPs at each locus in our DO mouse dataset. Within SNP plots at a single locus, we identified the region with the strongest association between individual SNPs and the phenotype by looking at regions until ∼1.5 LOD drop. For example, if SNPs have a LOD of 6.0, the significant region would span all genes with SNPs having a LOD of 4.5–6.0. For genes that were contained within these regions, we searched the IMPC resource for available phenotypes. Very few genes had live mice produced or plasma lipid phenotypes available. We also attempted to utilize single-tissue expression QTL datasets, including those for adipose and liver. However, for most lipoprotein QTL, we had difficulty identifying single-tissue expression QTL with allele effect patterns that matched those of our study QTL. Therefore, we chose to employ an analogous method of surveying syntenic regions in human GWAS for significant associations to cardiometabolic traits. A 2 Mbp region flanking the lipoprotein QTL was used to identify orthologous regions in the human genome using the LiftOver utility from UCSC Genomic Institute (genome.ucsc.edu/cgi-bin/hgLiftOver), and synteny was confirmed using the online Cinteny tool (24). Single nucleotide variants for cardiometabolic traits in these syntenic regions were harvested from GWAS Central (www.gwascentral.org) (25). By incorporating data from mouse SNPs, available mouse phenotyping, human single nucleotide variants, and searching literature for known roles in lipoprotein biology, candidate causal genes were nominated.

RT-PCR

For liver gene analyses, liver samples were homogenized in Qiazol lysis buffer in a TissueLyser II and RNA isolated with RNeasy Mini Kit (Qiagen) following the manufacturer's protocols. Hepatic gene expression of *Asah2* was normalized to β-actin (*Actb*), and fold change relative to wild-type controls for each sex was calculated using the $2^{-\Delta\Delta Ct}$ method (26).

Asah2 primer sequences: GATCCATTC TGGGACACTCTTC (forward), TCCACTGTGAAGCAGGATTG (reverse). *Actb* primer sequences: AGATGTGGATCAGCAAGCAGG (forward), TGCGCAAGTTAGGTTTTGTCA (reverse).

Statistical analyses

Founder plasma lipoprotein data were analyzed in JMP Pro, version 15.0.0 (SAS Institute, Cary, NC). All data were log-transformed prior to statistical analysis. Chow-fed and HFHS-fed data were initially analyzed separately for strain and sex effects, prior to assessing the interaction effect of diet on strain and sex. Strain, sex, and diet interactions for each lipoprotein subclass were tested using a standard least squares model with $P < 0.05$ denoting a significant effect. Least square means differences with Tukey's honest significant difference post hoc analysis determined statistical differences between groups ($P < 0.05$). For instances where the interaction effect and one of the main effects failed to reach significance, a one-way ANOVA was used. Heritability calculations were conducted in R (version 4.3.1) using the "lme4" package to fit a linear mixed model with restricted maximum likelihood. Chow-fed and HFHS-fed mice were analyzed separately, with sex as the fixed effect and strain as the variable effect. *Asah2* mouse data were first checked for a Gaussian distribution and log-transformed if not normally distributed. Statistical analyses of normally distributed data were performed by ANOVA followed by Tukey's post hoc analysis. Differences were considered significant at $P < 0.05$.

RESULTS

Strain and sex dependence of diet-induced alterations in lipoproteins

To estimate heritability (h^2) of lipoprotein phenotypes in DO mice, we first analyzed the lipoproteins of the eight founder strains of DO mice. The mice were fed a chow diet or a HFHS diet, and their plasma were analyzed by ion mobility analysis, a method that quantitates the various size categories of lipoproteins (supplemental Table S1) (27).

Mice fed a standard chow diet showed marked strain-dependent differences in their lipoprotein size distribution (**Fig. 1**A and supplemental Fig. S1), with significant interactions between strain and sex for all lipoprotein subclasses ($P < 0.03$). NOD, NZO, and PWK mice had increased lipoprotein abundance relative to the other strains ($P < 0.005$), with NZO having the highest concentrations of small LDL (LDL-IVa, -IVb,

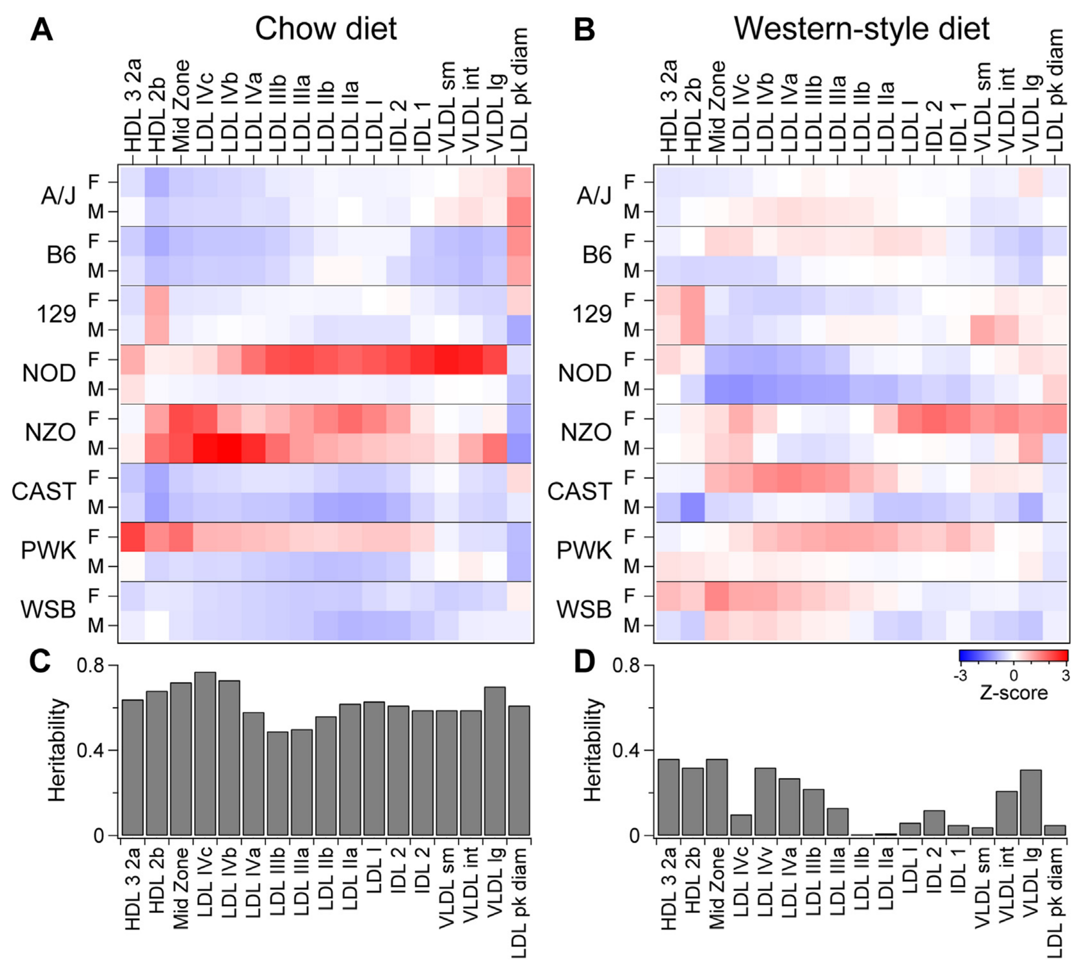

Fig. 1. Genetics and diet exert a strong influence on circulating lipoproteins. Profile of lipoprotein subclasses in female (F) and male (M) mice of the eight DO founder strains maintained on standard rodent chow diet (A) or a Western-style diet high in fat and sucrose (B). Heritability (h^2) estimates for lipoprotein particles in mice fed a chow diet (C) versus a Western-style diet (D).

-IVc, $P < 0.0001$). PWK mice showed variation in classes by sex where females (F) had increased the small lipoprotein particles: HDL-3,2a, HDL-2b, and midzone relative to male (M) PWK mice ($P < 0.007$, $P < 0.0001$, $P < 0.0001$, respectively). NZO mice had increased concentrations of LDL particles compared with the other strains ($P < 0.0001$), whereas B6, WSB, and CAST mice had the lowest LDL particle concentrations ($P < 0.03$). Heritability was high for all particles, with strain explaining up to 77% of phenotypic variance (Fig. 1C, $h^2 = 0.49–0.77$).

When placed on the HFHS diet for 16 weeks, total lipoprotein concentrations were increased by ~50% (25 ± 1 nM) in five of the eight mouse strains, compared with chow-fed mice (17 ± 1 nM, $P < 0.0001$). NZO, NOD, and PWK mice did not significantly change their total lipoprotein particle concentrations in response to the HFHS diet. However, there was no effect of sex or interaction between sex and strain on any of the individual subclasses in response to the HFHS diet (Fig. 1B and supplemental Fig. S1, $P > 0.3$). Therefore, we analyzed the particles by one-way ANOVA to determine differences between strains.

NOD mice had the lowest LDL-IIIb and LDL-IV particle concentrations relative to the other strains ($P < 0.001$). Large LDL-I and LDL-II particles did not vary by strain ($P > 0.5$). HDL-2b concentrations were highest in 129 mice and significantly different from CAST ($P < 0.0004$). Interestingly, the average LDL diameter was higher in chow-fed mice (204 ± 1 Å) compared with HFHS-fed mice (194 ± 1 Å, $P < 0.0001$). LDL peak diameter showed a strong strain dependence for chow-fed mice ($P < 0.0001$) that was not present for HFHS-fed mice ($P > 0.6$). Two mouse strains, A/J and B6, had the largest LDL diameter on the chow diet ($P < 0.0001$) but were not different from other strains on HFHS diet. Heritability for lipoprotein particle concentrations was diminished on the HFHS diet (Fig. 1D), with strain explaining ~40% or less of the variance in particle concentrations ($h^2 = 0–0.36$).

Genetic association of lipoprotein classes in DO mice

We surveyed all lipoprotein subclasses in ~500 DO mice genotyped at ~69,000 genome-wide SNPs, enabling us to identify 30 QTL with LOD >6.0 (genome-wide $P = 0.2$) for association with plasma lipoprotein subclasses (**Fig. 2**A and supplemental Table S2). For several QTL, multiple lipoproteins comapped, including one on chromosome 10 (Chr 10) for LDL-I through LDL-IIIb.

Because DO mice derive from an outcross of eight founder strains, there are up to eight alleles segregating among DO mice across the genome. Through haplotype reconstruction, we could determine the association of strain-specific haplotype blocks with each phenotype and thus determine the directionality of each allele's influence on the phenotype, that is, their allele signatures. Figure 2B illustrates the allele signatures for all lipoprotein QTLs.

We defined lipoprotein QTL based on the genome location of the SNP having the highest LOD score and the allele signatures of comapping traits. For example, a single locus on Chr 10 at ~57 Mbp that showed five LDL subclasses comapping in response to the same allele signature (low for B6 and high for 129 and WSB) was classified as a single QTL. After refining QTL based on genomic proximity and allele effects, we identified 21 unique QTL for all lipoprotein classes. Six QTL were identified for HDL-2b and five QTL for the HDL-2a,3 subclasses, the most for individual subclasses in our analyses (supplemental Table S2). Large VLDL had four QTL, whereas the remaining subclasses had 1–2 QTL.

To nominate causal genes at each QTL, we identified probable genes based on SNP association plots at each locus. One lipoprotein subclass, HDL-2b, significantly mapped to six loci, with four QTL having a LOD >6.0 (**Fig. 3**A). Each locus had a unique allele signature (Fig. 3B), indicating independent genetic regulation of this lipoprotein. By integrating mouse SNPs at each locus (supplemental Fig. S2 and supplemental Table S3), candidate genetic drivers were identified. The QTL on Chr 1 was located near *Apoa2*, the second most abundant apolipoprotein component of HDL (28). The QTL on Chr 9 was located near several apolipoproteins, including apolipoprotein A1 (*Apoa1*) as well as proprotein convertase subtilisin/kexin type 7 (*Pcsk7*). APOA1 is the most abundant apolipoprotein in HDL (28, 29) and has been well characterized for its role in HDL function (30). The association of three genetic variants of *PCSK7* with HDL-C and acute coronary syndrome has also been recently published (31).

Finding QTL at the *Apoa2* and *Apoa1/Pcsk7* loci demonstrated that our genetic screen could identify known drivers of cholesterol and lipoprotein levels. We next turned our attention to two distinct HDL-2b QTL on Chr 19. The first QTL includes a region between clusters of fatty acid desaturases (*Fads1*, *Fads2*, and *Fads3*) and membrane-spanning 4A (*Ms4a*) gene members (supplemental Fig. S2C), which have literature support for associations to lipid metabolism, total cholesterol, and HDL-C (32–34). The second QTL, on Chr 19, included two compelling genes (supplemental Fig. S2D): *N*-acylsphingosine amidohydrolase 2 (*Asah2*) and Apobec1 complementation factor (*A1cf*). Due to associations of ceramides with cardiovascular disease (35), we sought to investigate *Asah2*, which encodes a ceramide-catabolizing neutral ceramidase, as a causal gene for HDL-2b lipoproteins.

Validation of *Asah2* as a novel driver of plasma lipoprotein classes

To validate *Asah2* as a driver of HDL lipoproteins, whole-body *Asah2* knockout ($Asah2^{-/-}$), heterozygous

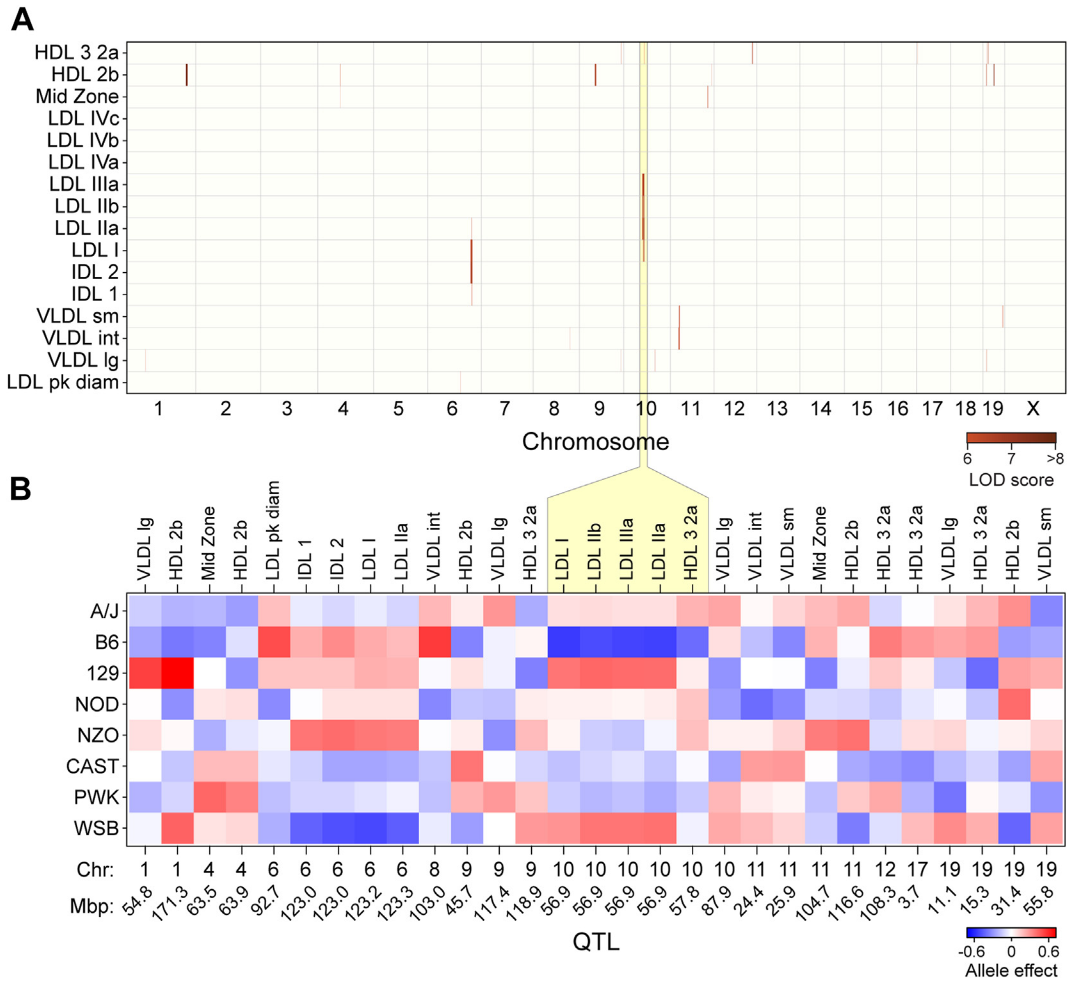

Fig. 2. Genetic architecture of circulating lipoproteins. Heatmaps illustrate average Z-scores across all mice for 3–5 mice per sex/strain. Genome-wide QTL for lipoprotein subclasses in ~500 DO mice maintained on Western-style diet (A). LODs greater than 7.4 met the genome-wide threshold for significant QTL, whereas LODs greater than 6.0 are considered suggestive QTL. Supplemental Table S2 lists all QTL, their genomic positions, LOD scores, and allele effect values. Allele effect values are illustrated for 30 QTL for individual lipoprotein subclasses (B). Blue depicts alleles associated with reduced lipoprotein values, red depicts for increased values. Founder strains are listed on the left, whereas lipoproteins and their QTL (Chr and Mbp location) are shown along the top and bottom, respectively. Loci with similar allele effect patterns (e.g., Chr 10 at ~57 Mpb for LDLIIIb–LDLIIa and HDL-3,2a) are considered one QTL.

(*Asah2*$^{+/-}$), or wild-type (*Asah2*$^{+/+}$) mice were fed a HFD for 16 weeks, and plasma was collected at 25 weeks of age. Loss of *Asah2* gene expression was confirmed in liver tissues of mice from each sex and genotype (supplemental Fig. S3). To assess potential shifts in lipoprotein classes, we used ion mobility analysis to measure lipoprotein concentrations by size. Overall, female *Asah2*$^{-/-}$ mice had increased levels of all lipoproteins compared with female *Asah2*$^{+/+}$ mice, with significant increases in HDL and IDL subclasses (**Fig. 4** and supplemental Fig. S4, $P < 0.01$). Specifically, female *Asah2*$^{-/-}$ had significantly higher concentrations of small HDL-3,2a (Fig. 4A, $P < 0.009$) and strong trends for large HDL-2b (Fig. 4B, $P < 0.07$) particles. Both male and female *Asah2*$^{-/-}$ mice showed trends for increased particles in the midzone size range compared with *Asah2*$^{+/+}$ mice ($P < 0.08$, $P < 0.09$, respectively). Three LDL subclasses, LDL-IIB (Fig. 4D), LDL-IIa (Fig. 4E), and LDL-1 (Fig. 4F), were increased in female *Asah2*$^{-/-}$ versus *Asah2*$^{+/+}$ mice. Similarly, IDL-2 (Fig. 4G) and IDL-1 (Fig. 4H) were more abundant in female *Asah2*$^{-/-}$ mice ($P < 0.008$). LDL-IIa, LDL-1, and both IDL particle classes were increased in female *Asah2*$^{-/-}$ versus *Asah2*$^{+/-}$ mice ($P < 0.04$), highlighting a gene dosage effect for these particles. Finally, small VLDL (Fig. 4I) was also increased in female *Asah2*$^{-/-}$ compared with *Asah2*$^{+/+}$ mice ($P < 0.03$). LDL, IDL, and VLDL particle subclasses were not different between genotypes in male mice.

Given the increased concentration of apo-B-containing particles in *Asah2*$^{-/-}$ mice, we asked if the abundance of the LDL receptor (LDLR) protein or mRNA was altered in *Asah2*$^{-/-}$ mice. We assessed LDLR protein in liver by Western blot. In *Asah2*$^{-/-}$ females, there was a small, but statistically significant, increase in LDLR protein compared with *Asah2*$^{+/+}$ females (supplemental Fig. S4F, H); males were not different by

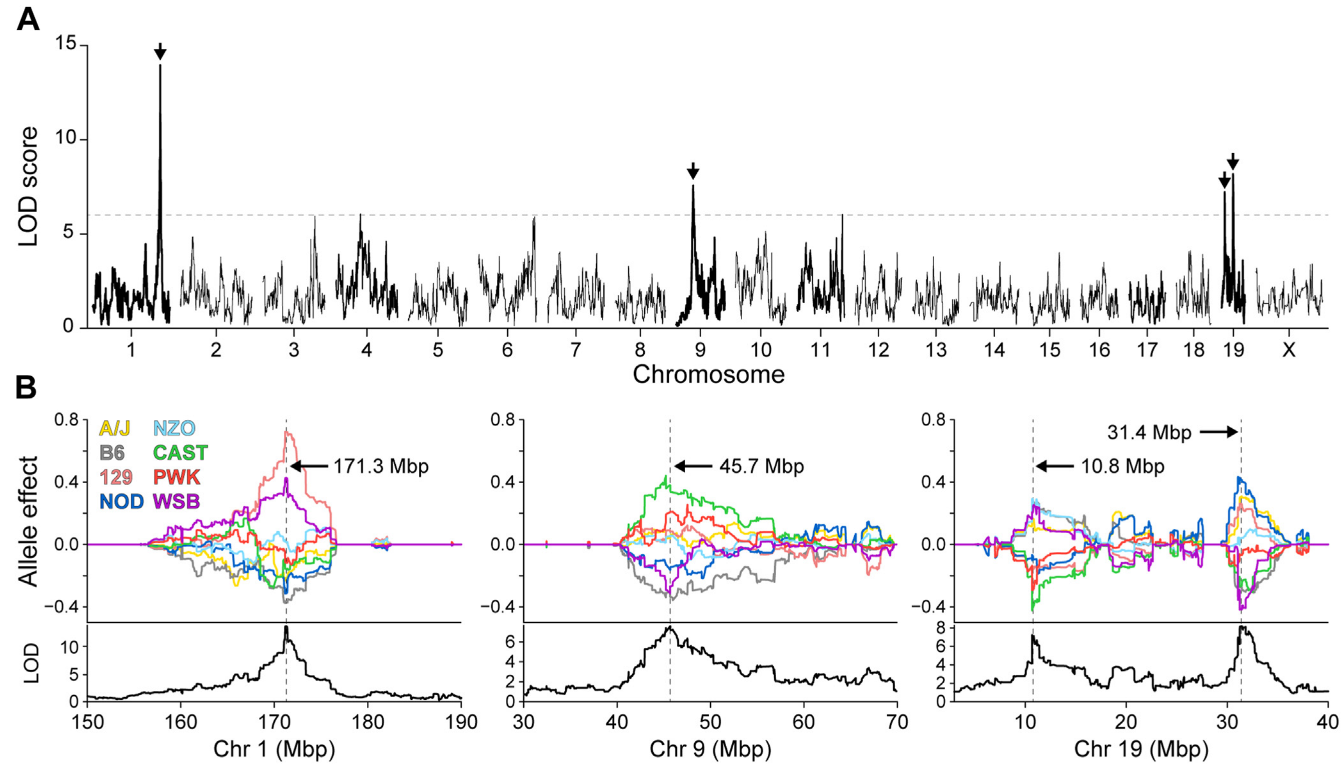

Fig. 3. Genetic regulation of circulating HDL-2b. Genome-wide LOD profile for an HDL subclass (HDL-2b) identifies significant QTL on three chromosomes: 1, 9, and 19 (A). Allele effect plots illustrate distinct genetic architecture at each locus (B). Colored lines represent alleles derived from founder strains. Genomic position for peak SNP listed for each QTL.

genotype (supplemental Fig. S4G, H). In addition, *Ldlr* and *Pcsk9* expression in liver was similar between genotypes of the same sex (supplemental Fig. S4I). Thus, the mechanism by which the loss of *Asah2* drives increased lipoprotein abundance is likely not because of downregulation of the LDLR protein.

Integration of mouse lipoprotein QTL with human GWAS

To determine the translational significance of our findings to humans, we analyzed the syntenic loci for significant traits in human GWAS. To determine synteny, a 2 Mbp flanking region was first identified for each mouse lipoprotein QTL. This 2 Mbp region was then used with the LiftOver utility from UCSC Genomic Institute (genome.ucsc.edu/cgi-bin/hgLiftOver) to yield the human syntenic locus for each QTL (supplemental Table S4). Synteny was further verified using the online Cinteny tool (24). We then asked if these loci were associated with cardiometabolic phenotypes, including cardiovascular, glycemic, blood lipid, or anthropometric (excluding height) traits in GWAS Central (www.gwascentral.org) (25).

Approximately 2,000 SNPs with cardiometabolic traits were identified within the syntenic regions (supplemental Table S5). SNPs syntenic with 20 of the 21 lipoprotein QTL identified in mice were strongly associated with metabolic traits in human GWAS ($P < 10^{-8}$, **Fig. 5**). Fifteen of the 21 loci were highly enriched with associations for three or more trait categories surveyed, providing evidence of significant genetic associations in the human population.

To nominate causal genes for each locus, we considered lipid-associated SNPs in mouse and human data and searched for literature support and mouse phenotyping data through the IMPC (www.mousephenotype.org). At mouse QTL, we prioritized SNPs that fell within the genomic region with a 1.5 LOD drop. At the syntenic loci in human, we identified SNPs with significant associations ($P < 10^{-8}$). Next, we searched published literature for phenotypic or mechanistic support. Through this integrated pipeline of mouse lipoprotein QTL, human GWAS data, and published publicly available data, we nominated candidate driver genes for 18 of the 21 lipoprotein QTL (Table 1).

We identified *Akna* as the candidate gene for HDL-2b and Midzone lipoprotein classes at a QTL on Chr 4. *Akna*, an AT-hook transcription factor (36), promotes *Cd40* expression (37), indicating a role in inflammatory processes. In human genetic association studies, *AKNA* variants have been linked to total cholesterol (38), HDL-C, and ApoA1 (39), and plasma sphingolipids (40). However, no studies have mechanistically linked *Akna* to cholesterol or lipoprotein metabolism. It is possible that *Akna* may reflect the role of HDL in inflammation and/or immune surveillance.

The second candidate driver for the HDL-2b locus on Chr 19 at ~32 Mbp is *A1cf* (Apobec1 complementation

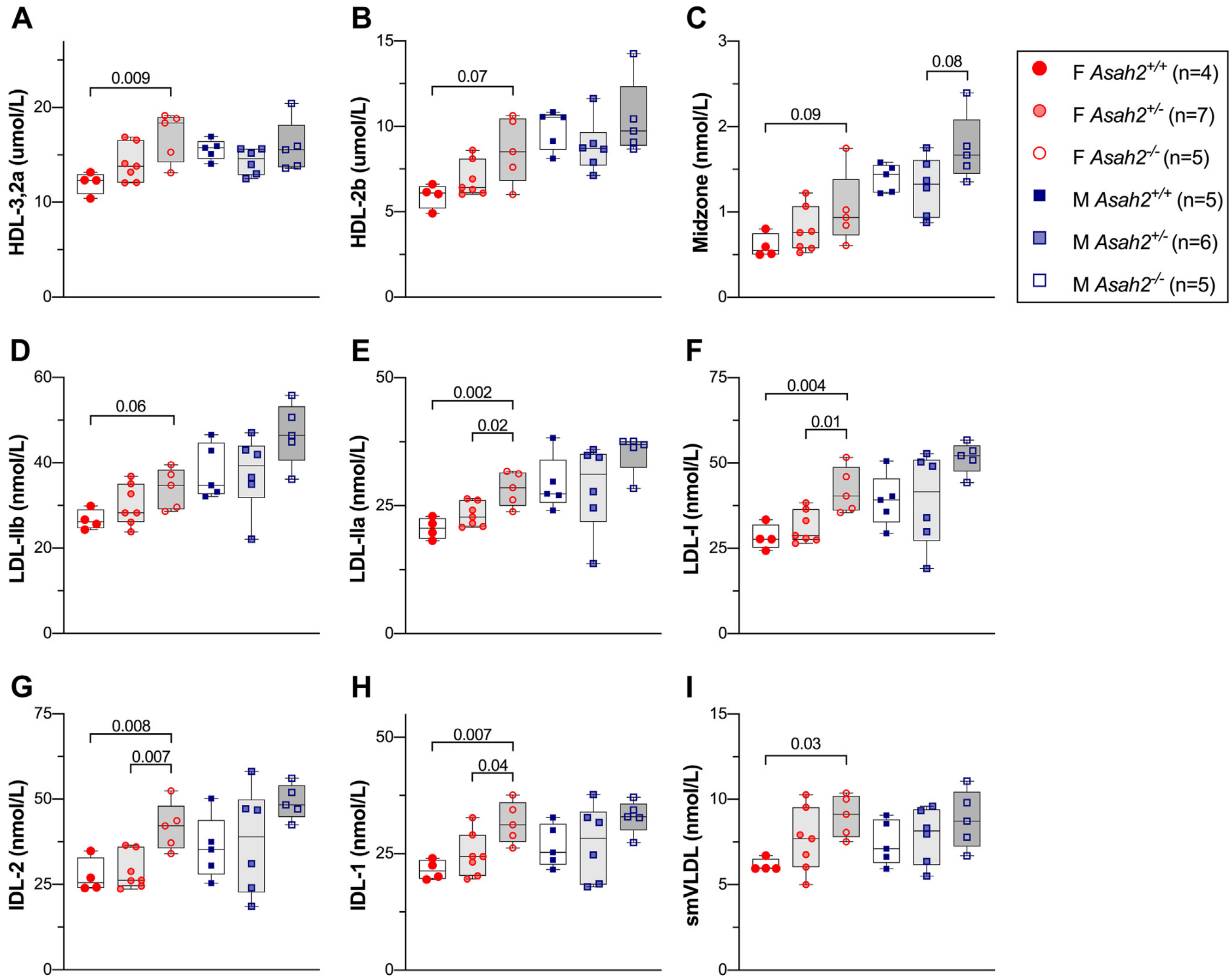

Fig. 4. *Asah2* is a driver of plasma lipoproteins in female mice. Circulating lipoprotein subclasses measured by ion mobility analysis in female and male $Asah2^{-/-}$, $Asah2^{-/+}$, and $Asah2^{+/+}$ mice. A: Small HDL-3,2a (76.5–105 Å) and (B) large HDL-2b (105–145 Å) concentrations were increased in $Asah2^{-/-}$ females. C: Both male and female $Asah2^{-/-}$ showed a trend for increased particles in the midzone size range (145–180 Å) compared with their $Asah2^{+/+}$ mice. Three LDL subclasses, LDL-IIB (D), LDL-IIa (E), and LDL-1 (F), two IDLs, IDL-2 (G) and IDL-1 (H), and small VLDL particles (I) were all elevated in $Asah2^{-/-}$ female mice.

factor). *A1cf* works in conjunction with *Apobec1* to catalyze the editing of *Apob* mRNA, which results in the introduction of a stop codon and production of a truncated protein product, ApoB48 (41, 42). In human GWAS, there are strong associations between *A1CF* missense variants and plasma lipoprotein phenotypes

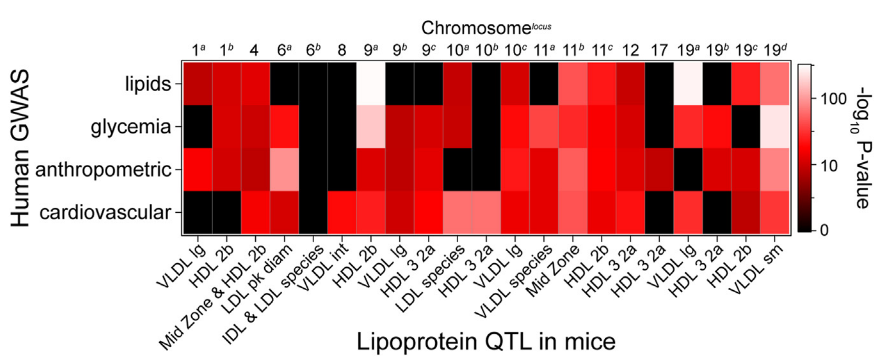

Fig. 5. Mouse lipoprotein QTL are syntenic to regions associated with cardiometabolic traits in humans. Heatmap illustrates maximum enrichment ($-\log_{10}$ *P* value) for single nucleotide polymorphisms that are present within regions syntenic to mouse lipoprotein QTL and associated with lipid, glycemia, anthropometric (excluding height), or cardiovascular phenotypes in human GWAS.

TABLE 1. Candidate genes for plasma lipoprotein QTL

Mouse		Human			
Phenotype	QTL Chr:Mbp	Syntenic locus Chr:Mbp	Lipid GWAS trait	*P*	Candidate gene(s)
HDL-3,2a	9:118.8	3:38.0	Phospholipids[a]	2×10^{-8}	*ITGA9*
	10:57.7	6:122.6	TC, HDL[a]	2×10^{-8}	*GJA1*
	12:108.3	14:100.0	TG[a]	4×10^{-10}	*CYP46A1, SLC25A47*
	17:3.6	6:155.9	HDL[b]	7×10^{-9}	*TIAM2*
	19:15.2	9:81.5	TC, LDL[b]	9×10^{-9}	*TLE4*
HDL-2b	1:171.2	1:161.2	TC[a]	1×10^{-11}	*APOA2*
	4:63.5	9:117.2	TC, HDL[a]	2×10^{-13}	*AKNA*
	9:45.6	11:117.3	TC, HDL, and TG[a]	1×10^{-300}	*APOA1*
	11:116.6	17:74.6	TC, LDL[a]	1×10^{-23}	*H3F3B*
	19:11.1	11:60.4	Fatty acids, ω-6[a]	4×10^{-274}	*FADS/MS4A* gene clusters
	19:31.4	10:53.3	TC, HDL, and TG[a]	2×10^{-25}	*A1CF*[c], *ASAH2*
Midzone	4:63.5	9:117.2	TC, HDL[a]	2×10^{-8}	*AKNA*[c]
	11:104.7	17:52.4	TC, LDL[a]	2×10^{-8}	*NPEPPS, KPBN1*
LDL species	6:122.9	12:8.1	N/A		*APOBEC1*
	10:56.8	6:122.2	TC, HDL[a]	2×10^{-8}	*GJA1*
IDL species	6:122.9	12:8.1	N/A		*APOBEC1*
VLDL species	11:24.3	2:60.5	TC, TG[b]	4×10^{-9}	
SmVLDL	19:55.7	10:114.7	TC, HDL[a]	3×10^{-64}	*GPAM*[c]
intVLDL	8:102.9	16:65.3	LDL[b]	9×10^{-11}	*CDH11*
lgVLDL	1:54.7	2:198.0	TC, HDL[a]	5×10^{-9}	*ANKRD44*
	9:117.3	3:29.1	N/A		
	10:87.9	12:102.8	TC, LDL[b]	1×10^{-15}	*IGF1*
	19:11.1	11:60.4	Fatty acids, ω-6[a]	4×10^{-274}	*FADS/MS4A* gene clusters
LDL diameter	6:92.7	3:64.5	TC[a]	4×10^{-8}	*ADAMTS9*

N/A, no significant associations to lipid traits in human GWAS; TC, total cholesterol; TG, triglyceride.
[a]From GWAS Central.
[b]From type 2 diabetes knowledge portal.
[c]Missense variant.

(total cholesterol, LDL-C, and serum ApoB) (25, https://t2d.hugeamp.org/).

We identified a single locus associated with both IDL and LDL, mapping to Chr 6 (Figs. 1, 2). Interestingly, when we looked at the syntenic locus in humans, there were no significant associations for cardiovascular, lipid, anthropometric, or glycemic traits. However, both the mouse and human genomic region contain *Apobec1* (apolipoprotein B mRNA-editing enzyme catalytic subunit 1). A recent study in DO mice also identified a QTL for atherosclerotic lesions at this locus (43). In *Apobec1*$^{-/-}$ mice, plasma ApoB-100 is increased 176%, although this was not accompanied by changes to cholesterol concentrations in VLDL or LDL classes (44). The lack of genetic association in humans may be due to species differences where mice express *Apobec1* in both liver and intestine (45), whereas human expression is restricted to the intestine (https://gtexportal.org/home/). It may also highlight the minimal contribution of plasma ApoB-48 concentration to total ApoB and the poor correlation to plasma cholesterol in humans (46, 47).

We mapped a single locus spanning five LDL subclasses (Chr 10) and one for LDL diameter (Chr 6). *Gja1*, also known as connexin 43 (*Cnx43*), is our candidate gene for the LDL species mapping to Chr 10. *Cnx43*$^{+/-}$/*Ldlr*$^{-/-}$ mice have a reduction in atherosclerotic lesion formation, compared with *Cnx43*$^{+/+}$/*Ldlr*$^{-/-}$ mice, without a change in plasma cholesterol or triglyceride (48). *Adamts9*, the candidate gene for LDL diameter, is a metallopeptidase with a type 1 thrombospondin motif. *Adamts9* has not been directly studied for a role in lipoprotein metabolism but has been shown to be a suppressor of mammalian target of rapamycin pathway in cancer cell lines (49). Both thrombospondin-1 and thrombospondin-2, however, have been studied in cardiovascular disease (50, 51) and mediate atherosclerotic plaque development in mice (52, 53).

We identified seven QTL for the three major size ranges within VLDL particles. At these loci, we identified five candidate genes. Small VLDL, which mapped to Chr 19, includes the gene *Gpam* at the human syntenic locus. In mice, the founder strains CAST and PWK have splice and untranslated region variants (supplemental Table S5), consistent with those two strains carrying the low alleles for the Chr 19 QTL (supplemental Table S1). Within human GWAS, *GPAM* is strongly associated with HDL, LDL, and total cholesterol, with missense variants that are highly associated to each of the three traits (supplemental Table S4, https://t2d.hugeamp.org/). *Gpam* encodes for outer mitochondrial membrane glycerol-3-phosphate acyltransferase, an enzyme in the triglyceride synthesis pathway. Consistent with a role in lipoprotein metabolism, *Gpam* knockout mice have lower VLDL secretion rates and decreased liver triglycerides relative to wild-type mice (54).

We nominate *Igf1* as the causal gene at a QTL on Chr 10 for large VLDL. In mice, *Igf1* was shown to reduce liver cholesterol accumulation by activating *Abca1* (55), and an association between plasma *Igf1* cardiovascular disease risk has been found in human subjects (56). In bovine hepatocytes, *Apob* expression and VLDL secretion are increased with addition of exogenous IGF1 (57).

For two additional VLDL QTL (Chrs 1 and 8), we identified two lesser-known gene candidates: *Ankrd44* and *Cdh11*, respectively. In a study looking for genetic drivers of stroke in cerebral arteries, *Ankrd44* was downregulated in veins from rabbits with hypercholesterolemia alone and with combined hypercholesterolemia and hypertension (58). *ANKRD44* genetic variants are associated with stroke risk in African Americans (59), though no mechanistic studies were found. Cadherin-11 (*Cdh11*), a cell adhesion protein, was nominated as the causal gene for intermediate-sized VLDL mapping to Chr 8. *Cdh11* has been implicated in autoimmune disorders, aortic valve calcification, and recently, scarring following myocardial infarction through its effect on fibrosis and inflammation (60). In a mouse model of atherosclerosis, *Cdh11* expression was increased in atherosclerotic plaques of $ApoE^{-/-}$ mice. $ApoE^{-/-}/Cdh11^{-/-}$ double knockout mice had altered immune cell populations and increased atherosclerosis (61).

DISCUSSION

Lipoproteins that are isolated based on size or buoyant density represent snapshots of dynamic processes involving the transfer of lipids and proteins between particles and between tissues and lipoprotein particles. Genetic linkage and association studies help to identify the genes that affect these dynamic processes. The heterogeneity of the major lipoprotein classes (VLDL, LDL, and HDL) in the DO founder strains suggested that we might find QTL that explain this heterogeneity (Fig. 1).

Prior to embarking on the genetic study in DO mice, we first estimated heritability (h^2) of these distinct lipoprotein subclasses in the eight founder strains fed either chow diet or HFHS diet. Heritability estimates were reduced by approximately half for mice maintained on the HFHS diet (Fig. 1C, D), which in part may reflect increased intrastrain variance in particle concentrations (supplemental Fig. S1). Previous reports have highlighted an interaction between diet and genetics that alters heritability of metabolic phenotypes. In pedigreed baboons, high fat and/or high cholesterol diets increased variance and reduced h^2 in plasma HDL-C, median HDL size, and ApoA1/ApoB protein abundance compared with a low-fat, low-cholesterol diet (62). In a survey of 13 inbred mouse strains fed a Western diet, up to 75% of variance in lean body weight could be attributed to genetics (h^2), whereas other phenotypes (e.g., plasma glucose) showed reduced heritability ($h^2 < 20\%$) (63). Finally, a panel of 22 inbred CC strains showed that some traits (e.g., body weight and plasma cholesterol) showed higher variation than other traits (e.g., body fat) between high-protein diet or HFD (64). Our results are consistent with these previous findings, showing that a metabolically challenging diet can increase nongenetic variance and thus reduce estimated h^2 of metabolic phenotypes.

Despite the reduction in estimated heritability observed for mice maintained on the HFHS diet, we identified 21 QTL for 16 lipoprotein subclasses in DO mice. Some of the loci contain genes encoding well-known apolipoproteins (e.g., the locus harboring apoA1, C3, A4, A5, and PCSK7, and another locus containing apoA2), inspiring confidence in the ability of our screen to detect relevant loci. Nearly all these QTL, when lifted over into the human genome, are associated with lipid traits, as well as other cardiometabolic phenotypes, including cardiovascular disease risk, body weight, and diabetes.

At the HDL-2b locus on Chr 19 at ~32 Mbp, we identified two candidate drivers: *Asah2* and *A1cf*. We chose to investigate the relationship between *Asah2* and lipoproteins by phenotyping $Asah2^{-/-}$ mice. In female mice fed an HFD, *Asah2* deletion resulted in increased HDL, midzone, large LDL, IDL, and small VLDL particles (Fig. 4). A similar trend was seen in midzone and IDL-2 particles in male mice. *Asah2* is highly expressed in the intestine and functions as a neutral ceramidase. Although sphingolipids, including ceramides, can be carried on LDL and VLDL particles (65), to our knowledge, this is the first time a ceramidase has been shown to affect lipoprotein abundance.

Ceramides have recently been recognized as a cholesterol-independent lipid biomarker of cardiovascular disease risk (66), with the potential for being a predictor of endothelial dysfunction and early atherosclerosis (67). In a mouse model of atherosclerosis, pharmacological inhibition of hypoxia-inducible factor 1α in adipose tissue decreased ceramide formation through a neutral sphingomyelinase and was associated with decreased plasma cholesterol and delayed atherosclerotic plaque progression (68). Moreover, targeted disruption of ceramide synthesis similarly blunts plaque formation. Specifically, genetic deletion (69) or pharmacological inhibition (70, 71) of serine palmitoyltransferase, which catalyzes the committed step in de novo ceramide synthesis, also blunts plaque formation. *Asah2* is required for intestinal degradation of dietary sphingolipids (19). As *ASAH2* expression is predominantly in the intestine, its activity may alter intestinal absorption of cholesterol. Indeed, strategies that reduce ceramides in the gut can blunt cholesterol absorption (72, 73). Moreover, ASAH2 mediates the body's response to microbial sphingolipids (19, 74). Deletion of *Asah2* alleviates diet-induced nonalcoholic steatohepatitis/nonalcoholic fatty liver disease via downregulation of stearoyl-CoA desaturase (*Scd1*) and reduces cholesterol accumulation (75). When fed a very low-fat diet, $Scd1^{-/-}$ mice have increased plasma cholesterol, especially in the LDL and VLDL fractions (76). When fed a standard chow diet (13% calories as fat), *Scd1*$^{-/-}$ mice have increased plasma HDL-C (77). Therefore, one might hypothesize that *Asah2* modulates lipoprotein metabolism through its effect on *Scd1* expression.

For many years, elevated HDL was considered to be protective against atherosclerosis. However, Mendelian randomization studies and mouse knockout experiments showed that this concept was overly simplistic (78). Rather, opposing dynamic processes affect HDL and atherosclerosis risk by affecting the dynamics of cholesterol transport. For example, mutations in *ABCA1* reduce the ability of cells to transport cholesterol and phospholipids out of cells (79, 80). This results in lower HDL and increased atherosclerosis (81). In contrast, mutations in *SRB1* decrease the transport of cholesterol esters from HDL into cells (82–84). This leads to increased HDL and increased atherosclerosis.

We are not aware of any genetic association between *ASAH2* and atherosclerosis. Its modulation of HDL could increase or decrease atherosclerosis. Alternatively, *ASAH2* could affect atherosclerosis through its effects on sphingolipids, independent of its effect on HDL, through their effects on inflammatory pathways (85). Indeed, ceramides predict coronary artery disease independently of cholesterol (86). Pharmacological inhibition of ceramide synthesis via the serine palmitoyltransferase inhibitor, myriocin, reduces atherosclerotic plaque formation in APOE-deficient mice (71, 73). Moreover, ceramidases can also increase the formation of sphingosine-1-phosphate, an anti-atherogenic lipid that is largely carried in ApoM-containing particles (87).

Interestingly, a recent mouse genetic study identified a QTL for atherosclerotic lesions at the *Asah2* locus in male mice (88). This study utilized a DO-F1 mouse population, generated by breeding DO mice to cholesteryl ester transfer protein;ApoE3-Leiden mice to produce an F1 generation with increased susceptibility to atherosclerosis. While their QTL on Chr 18 overlapped in position with the *Asah2* locus in our study, the allele effects did not match between the two studies. It is possible that the discrepancies in allele effects are due to breeding strategies or reflective of differing responses to dietary compositions. Nevertheless, it is intriguing that this locus has been linked to both atherosclerosis and lipoprotein biology in two mouse genetic screens.

In summary, we mapped mouse lipoprotein subclasses to identify 21 unique QTL, which we then crossreferenced with the human syntenic locus to determine candidate genes associated with cardiometabolic traits in human GWAS. By integrating mouse data with human GWAS at the syntenic locus, we nominated candidate genes for 18 unique lipoprotein QTL. Deletion of *Asah2*, a novel candidate driver for HDL-2b, resulted in increased HDL, midzone, large LDL, IDL, and small VLDL particles in plasma from female mice. Similar validation experiments can be performed to explore the candidate genes we have nominated at the remaining QTL.

Data availability

Plasma lipoprotein raw data and R scripts used for this study are provided as supplemental data. DO mouse genotyping information has been previously published along with scripts for running the analyses on Unix shell and R scripts (22).

Supplemental data

This article contains supplemental data.

Acknowledgments

We appreciate the gift of *Asah2*$^{-/-}$ mice by Richard Proia (National Institutes of Health) to the Summers/Holland laboraory. We would like to thank Daniel Gatti and Gary Churchill at The Jackson Laboratory for writing the foundational R code on which we based our R scripts for heritability calculations and QTL analyses.

Author contributions

M. P. K. and A. D. A. conceptualization; T. R. P., S. K., and R. M. K. methodology; T. R. P., C. H. E., S. K., B. S. Y., and R. M. K. validation; T. R. P. formal analysis; K. L. S. and R. N. investigation; C. H. E., T. B., S. A. S., and W. L. H. resources; T. R. P. and B. S. Y. data curation; T. R. P. writing–original draft; C. H. E., R. N., T. B., S. A. S., W. L. H., M. P. K., and A. D. A. writing–review & editing; T. R. P. and M. P. K. visualization; M. P. K. and A. D. A. supervision; M. P. K. and A. D. A. project administration; A. D. A. funding acquisition.

Author ORCIDs

Tara R. Price https://orcid.org/0000-0001-6034-7952
Christopher H. Emfinger https://orcid.org/0000-0002-9130-4194
Kathryn L. Schueler https://orcid.org/0000-0003-4260-581X
Rebekah Nicholson https://orcid.org/0000-0001-8929-3580
Tim Beck https://orcid.org/0000-0002-0292-7972
Scott A. Summers https://orcid.org/0000-0002-4919-0592
Alan D. Attie https://orcid.org/0000-0002-0568-2261

Funding and additional information

This work was supported by grants from the National Institutes of Health (grant nos.: R01DK101573, R01DK102948, and RC2DK125961) (to A. D. A.) and by the University of Wisconsin-Madison, Department of Biochemistry and Office of the Vice Chancellor for Research and Graduate Education with funding from the Wisconsin Alumni Research Foundation (to M. P. K.). Research support to T. R. P. was provided through the National Institutes of Health by the Training Program in Translational Cardiovascular Science (grant no.: T32-HL007936) at UW-Madison. Support to C. H. E. was provided by the American Diabetes Association (grant no.: 7-21-PDF-157). The content is solely the responsibility of the authors and does not necessarily represent the official views of the National Institutes of Health.

Conflict of interest

The authors declare that they have no conflicts of interest with the contents of this article.

Abbreviations

CC, collaborative cross; Chr, chromosome; DO, diversity outbred; GWAS, genome-wide association study; HFHS, high-fat, high-sucrose diet; IMPC, International Mouse Phenotyping Consortium; LDLR, LDL receptor; LOD, logarithm of odds; NIH, National Institutes of Health; Pcsk7, proprotein convertase subtilisin–kexin type 7; QTL, quantitative trait loci; SNPs, single nucleotide polymorphisms.

Manuscript received August 30, 2023, and in revised form October 28, 2023. Published, JLR Papers in Press, November 7, 2023, https://doi.org/10.1016/j.jlr.2023.100471

REFERENCES

1. Krauss, R. M. (2010) Lipoprotein subfractions and cardiovascular disease risk. *Curr. Opin. Lipidol.* **21**, 305–311
2. Berneis, K., Rizzo, M., Spinas, G. A., Di Lorenzo, G., Di Fede, G., Pepe, I., *et al.* (2009) The predictive role of atherogenic dyslipidemia in subjects with non-coronary atherosclerosis. *Clin. Chim. Acta.* **406**, 36–40
3. Asztalos, B. F., Cupples, L. A., Demissie, S., Horvath, K. V., Cox, C. E., Batista, M. C., *et al.* (2004) High-density lipoprotein subpopulation profile and coronary heart disease prevalence in male participants of the Framingham Offspring Study. *Arterioscler. Thromb. Vasc. Biol.* **24**, 2181–2187
4. Mueller, O., Chang, E., Deng, D., Franz, T., Jing, D., Kincaid, R., *et al.* (2008) PROCAM Study: risk prediction for myocardial infarction using microfluidic high-density lipoprotein (HDL) subfractionation is independent of HDL cholesterol. *Clin. Chem. Lab. Med.* **46**, 490–498
5. Kontush, A. (2015) HDL particle number and size as predictors of cardiovascular disease. *Front. Pharmacol.* **6**, 218
6. Davidson, W. S., Silva, R. A. G. D., Chantepie, S., Lagor, W. R., Chapman, M. J., and Kontush, A. (2009) Proteomic analysis of defined HDL subpopulations reveals particle-specific protein clusters: relevance to antioxidative function. *Arterioscler. Thromb. Vasc. Biol.* **29**, 870–876
7. Gordon, S. M., Deng, J., Lu, L. J., and Davidson, W. S. (2010) Proteomic characterization of human plasma high density lipoprotein fractionated by gel filtration chromatography. *J. Proteome Res.* **9**, 5239–5249
8. Vaisar, T., Pennathur, S., Green, P. S., Gharib, S. A., Hoofnagle, A. N., Cheung, M. C., *et al.* (2007) Shotgun proteomics implicates protease inhibition and complement activation in the antiinflammatory properties of HDL. *J. Clin. Invest.* **117**, 746–756
9. Camont, L., Lhomme, M., Rached, F., Goff, W. L., Nègre-Salvayre, A., Salvayre, R., *et al.* (2013) Small, dense high-density lipoprotein-3 particles are enriched in negatively charged phospholipids relevance to cellular cholesterol efflux, antioxidative, antithrombotic, anti-inflammatory, and antiapoptotic functionalities. *Arterioscler. Thromb. Vasc. Biol.* **33**, 2715–2723
10. Leduc, M. S., Blair, R. H., Verdugo, R. A., Tsaih, S-W., Walsh, K., Churchill, G. A., *et al.* (2012) Using bioinformatics and systems genetics to dissect HDL-cholesterol genetics in an MRL/MpJ × SM/J intercross. *J. Lipid Res.* **53**, 1163–1175
11. Lyons, M. A., Korstanje, R., Li, R., Walsh, K. A., Churchill, G. A., Carey, M. C., *et al.* (2004) Genetic contributors to lipoprotein cholesterol levels in an intercross of 129S1/SvImJ and RIIIS/J inbred mice. *Physiol. Genomics.* **17**, 114–121
12. Lusis, A. J., Taylor, B. A., Quon, D., Zollman, S., and LeBoeuf, R. C. (1987) Genetic factors controlling structure and expression of apolipoproteins B and E in mice. *J. Biol. Chem.* **262**, 7594–7604
13. Lusis, A. J., Seldin, M. M., Allayee, H., Bennett, B. J., Civelek, M., Davis, R. C., *et al.* (2016) The Hybrid Mouse Diversity Panel: a resource for systems genetics analyses of metabolic and cardiovascular traits. *J. Lipid Res.* **57**, 925–942
14. Kang, E. Y., Han, B., Furlotte, N., Joo, J. W. J., Shih, D., Davis, R. C., *et al.* (2014) Meta-analysis identifies gene-by-environment interactions as demonstrated in a study of 4,965 mice. *PLoS Genet.* **10**, e1004022
15. de Conti, A., Tryndyak, V., Willett, R. A., Borowa-Mazgaj, B., Watson, A., Patton, R., *et al.* (2020) Characterization of the variability in the extent of nonalcoholic fatty liver induced by a high-fat diet in the genetically diverse collaborative cross mouse model. *FASEB J.* **34**, 7773–7785
16. Svenson, K. L., Gatti, D. M., Valdar, W., Welsh, C. E., Cheng, R., Chesler, E. J., *et al.* (2012) High-resolution genetic mapping using the mouse diversity outbred population. *Genetics.* **190**, 437–447
17. Keller, M. P., Rabaglia, M. E., Schueler, K. L., Stapleton, D. S., Gatti, D. M., Vincent, M., *et al.* (2019) Gene loci associated with insulin secretion in islets from nondiabetic mice. *J. Clin. Invest.* **129**, 4419–4432
18. Mitok, K. A., Freiberger, E. C., Schueler, K. L., Rabaglia, M. E., Stapleton, D. S., Kwiecien, N. W., *et al.* (2018) Islet proteomics reveals genetic variation in dopamine production resulting in altered insulin secretion. *J. Biol. Chem.* **293**, 5860–5877
19. Kono, M., Dreier, J. L., Ellis, J. M., Allende, M. L., Kalkofen, D. N., Sanders, K. M., *et al.* (2006) Neutral ceramidase encoded by the Asah2 gene is essential for the intestinal degradation of sphingolipids. *J. Biol. Chem.* **281**, 7324–7331
20. Musunuru, K., Orho-Melander, M., Caulfield, M. P., Li, S., Salameh, W. A., Reitz, R. E., *et al.* (2009) Ion mobility analysis of lipoprotein subfractions identifies three independent axes of cardiovascular risk. *Arterioscler. Thromb. Vasc. Biol.* **29**, 1975–1980
21. Mora, S., Caulfield, M. P., Wohlgemuth, J., Chen, Z., Superko, H. R., Rowland, C. M., *et al.* (2015) Atherogenic lipoprotein subfractions determined by ion mobility and first cardiovascular events after random allocation to high-intensity statin or placebo: the justification for the use of statins in prevention: an intervention trial evaluating rosuvastatin (JUPITER) trial. *Circulation.* **132**, 2220–2229
22. Linke, V., Overmyer, K. A., Miller, I. J., Brademan, D. R., Hutchins, P. D., Trujillo, E. A., *et al.* (2020) A large-scale genome-lipid association map guides lipid identification. *Nat. Metab.* **2**, 1149–1162
23. Churchill, G. A., and Doerge, R. W. (1994) Empirical threshold values for quantitative trait mapping. *Genetics.* **138**, 963–971
24. Sinha, A. U., and Meller, J. (2007) Cinteny: flexible analysis and visualization of synteny and genome rearrangements in multiple organisms. *BMC Bioinformatics.* **8**, 82
25. Beck, T., Shorter, T., and Brookes, A. J. (2019) GWAS central: a comprehensive resource for the discovery and comparison of genotype and phenotype data from genome-wide association studies. *Nucleic Acids Res.* **48**, D933–D940
26. Winer, J., Jung, C. K. S., Shackel, I., and Williams, P. M. (1999) Development and validation of real-time quantitative reverse transcriptase–polymerase chain reaction for monitoring gene expression in cardiac myocytes in vitro. *Anal. Biochem.* **270**, 41–49
27. Caulfield, M. P., Li, S., Lee, G., Blanche, P. J., Salameh, W. A., Benner, W. H., *et al.* (2008) Direct determination of lipoprotein particle sizes and concentrations by ion mobility analysis. *Clin. Chem.* **54**, 1307–1316
28. Pamir, N., Hutchins, P., Ronsein, G., Vaisar, T., Reardon, C. A., Getz, G. S., *et al.* (2016) Proteomic analysis of HDL from inbred mouse strains implicates APOE associated with HDL in reduced cholesterol efflux capacity via the ABCA1 pathway. *J. Lipid Res.* **57**, 246–257
29. Shah, A. S., Tan, L., Long, J. L., and Davidson, W. S. (2013) Proteomic diversity of high density lipoproteins: our emerging understanding of its importance in lipid transport and beyond. *J. Lipid Res.* **54**, 2575–2585
30. Kontush, A. (2014) HDL-mediated mechanisms of protection in cardiovascular disease. *Cardiovasc. Res.* **103**, 341–349
31. Vargas-Alarcón, G., Pérez-Méndez, O., González-Pacheco, H., Ramírez-Bello, J., Posadas-Sánchez, R., Escobedo, G., *et al.* (2021) The rs508487, rs236911, and rs236918 genetic variants of the proprotein convertase subtilisin–kexin type 7 (PCSK7) gene are associated with acute coronary syndrome and with plasma concentrations of HDL-cholesterol and triglycerides. *Cells.* **10**, 1444
32. Chang, Y. T., Mori, E., Suzuki, M., Ikeda, M., Huang, C. W., Lee, J. J., *et al.* (2019) APOE-MS4A genetic interactions are associated with executive dysfunction and network abnormality in clinically mild Alzheimer's disease. *Neuroimage Clin.* **21**, 101621
33. Dumont, J., Goumidi, L., Grenier-Boley, B., Cottel, D., Marécaux, N., Montaye, M., *et al.* (2018) Dietary linoleic acid interacts with

FADS1 genetic variability to modulate HDL-cholesterol and obesity-related traits. *Clin. Nutr.* **37**, 1683–1689
34. Hayashi, Y., Lee-Okada, H. C., Nakamura, E., Tada, N., Yokomizo, T., Fujiwara, Y., *et al.* (2021) Ablation of fatty acid desaturase 2 (FADS2) exacerbates hepatic triacylglycerol and cholesterol accumulation in polyunsaturated fatty acid-depleted mice. *FEBS Lett.* **595**, 1920–1932
35. Zietzer, A., Düsing, P., Reese, L., Nickenig, G., and Jansen, F. (2022) Ceramide metabolism in cardiovascular disease: a network with high therapeutic potential. *Arterioscler. Thromb. Vasc. Biol.* **42**, 1220–1228
36. Siddiqa, A., Sims-Mourtada, J. C., Guzman-Rojas, L., Rangel, R., Guret, C., Madrid-Marina, V., *et al.* (2001) Regulation of CD40 and CD40 ligand by the AT-hook transcription factor AKNA. *Nature.* **410**, 383–387
37. Suram, S., Silveira, L. J., Mahaffey, S., Brown, G. D., Bonventre, J. V., Williams, D. L., *et al.* (2013) Cytosolic phospholipase A2α and eicosanoids regulate expression of genes in macrophages involved in host defense and inflammation. *PLoS One.* **8**, e69002
38. Klarin, D., Damrauer, S. M., Cho, K., Sun, Y. V., Teslovich, T. M., Honerlaw, J., *et al.* (2018) Genetics of blood lipids among ~300, 000 multi-ethnic participants of the Million Veteran program. *Nat. Genet.* **50**, 1514–1523
39. Richardson, T. G., Sanderson, E., Palmer, T. M., Ala-Korpela, M., Ference, B. A., Davey Smith, G., *et al.* (2020) Evaluating the relationship between circulating lipoprotein lipids and apolipoproteins with risk of coronary heart disease: a multivariable Mendelian randomisation analysis. *PLoS Med.* **17**, e1003062
40. Montasser, M. E., Aslibekyan, S., Srinivasasainagendra, V., Tiwari, H. K., Patki, A., Bagheri, M., *et al.* (2022) An Amish founder population reveals rare-population genetic determinants of the human lipidome. *Commun. Biol.* **5**, 334
41. Fossat, N., Tourle, K., Radziewic, T., Barratt, K., Liebhold, D., Studdert, J. B., *et al.* (2014) C to U RNA editing mediated by APOBEC1 requires RNA-binding protein RBM47. *EMBO Rep.* **15**, 903–910
42. Nikolaou, K. C., Vatandaslar, H., Meyer, C., Schmid, M. W., Tuschl, T., and Stoffel, M. (2019) The RNA-binding protein A1CF regulates hepatic fructose and glycerol metabolism via alternative RNA splicing. *Cell Rep.* **29**, 283–300.e8
43. Smallwood, T. L., Gatti, D. M., Quizon, P., Weinstock, G. M., Jung, K-C., Zhao, L., *et al.* (2014) High-resolution genetic mapping in the diversity outbred mouse population identifies Apobec1 as a candidate gene for atherosclerosis. *G3 (Bethesda).* **4**, 2353–2363
44. Nakamuta, M., Chang, B. H-J., Zsigmond, E., Kobayashi, K., Lei, H., Ishida, B. Y., *et al.* (1996) Complete phenotypic characterization of apobec-1 knockout mice with a wild-type genetic background and a human apolipoprotein B transgenic background, and restoration of apolipoprotein B mRNA editing by somatic gene transfer of Apobec-1. *J. Biol. Chem.* **271**, 25981–25988
45. Schaum, N., Karkanias, J., Neff, N. F., May, A. P., Quake, S. R., Wyss-Coray, T., *et al.* (2018) Single-cell transcriptomics of 20 mouse organs creates a Tabula Muris. *Nature.* **562**, 367–372
46. Otokozawa, S., Ai, M., Diffenderfer, M. R., Asztalos, B. F., Tanaka, A., Lamon-Fava, S., *et al.* (2009) Fasting and postprandial apolipoprotein B-48 levels in healthy, obese, and hyperlipidemic subjects. *Metabolism.* **58**, 1536–1542
47. Sakai, N., Uchida, Y., Ohashi, K., Hibuse, T., Saika, Y., Tomari, Y., *et al.* (2003) Measurement of fasting serum apoB-48 levels in normolipidemic and hyperlipidemic subjects by ELISA1. *J. Lipid Res.* **44**, 1256–1262
48. Kwak, B. R., Veillard, N., Pelli, G., Mulhaupt, F., James, R. W., Chanson, M., *et al.* (2003) Reduced Connexin43 expression inhibits atherosclerotic lesion formation in low-density lipoprotein receptor–deficient mice. *Circulation.* **107**, 1033–1039
49. Du, W., Wang, S., Zhou, Q., Li, X., Chu, J., Chang, Z., *et al.* (2013) ADAMTS9 is a functional tumor suppressor through inhibiting AKT/mTOR pathway and associated with poor survival in gastric cancer. *Oncogene.* **32**, 3319–3328
50. Bai, J., Xia, M., Xue, Y., Ma, F., Cui, A., Sun, Y., *et al.* (2020) Thrombospondin 1 improves hepatic steatosis in diet-induced insulin-resistant mice and is associated with hepatic fat content in humans. *EBioMedicine.* **57**, 102849
51. Zhang, K., Li, M., Yin, L., Fu, G., and Liu, Z. (2020) Role of thrombospondin-1 and thrombospondin-2 in cardiovascular diseases (review). *Int. J. Mol. Med.* **45**, 1275–1293
52. Maimaitiyiming, H., Clemons, K., Zhou, Q., Norman, H., and Wang, S. (2015) Thrombospondin1 deficiency attenuates obesity-associated microvascular complications in ApoE-/- mice. *PLoS One.* **10**, e0121403
53. Ganguly, R., Khanal, S., Mathias, A., Gupta, S., Lallo, J., Sahu, S., *et al.* (2021) TSP-1 (thrombospondin-1) deficiency protects ApoE−/− mice against leptin-induced atherosclerosis. *Arterioscler. Thromb. Vasc. Biol.* **41**, e112–e127
54. Hammond, L. E., Gallagher, P. A., Wang, S., Hiller, S., Kluckman, K. D., Posey-Marcos, E. L., *et al.* (2002) Mitochondrial glycerol-3-phosphate acyltransferase-deficient mice have reduced weight and liver triacylglycerol content and altered glycerolipid fatty acid composition. *Mol. Cell. Biol.* **22**, 8204–8214
55. Fukunaga, K., Imachi, H., Lyu, J., Dong, T., Sato, S., Ibata, T., *et al.* (2018) IGF1 suppresses cholesterol accumulation in the liver of growth hormone-deficient mice via the activation of ABCA1. *Am. J. Physiol. Endocrinol. Metab.* **315**, E1232–E1241
56. Succurro, E., Arturi, F., Grembiale, A., Iorio, F., Laino, I., Andreozzi, F., *et al.* (2010) Positive association between plasma IGF1 and high-density lipoprotein cholesterol levels in adult nondiabetic subjects. *Eur. J. Endocrinol.* **163**, 75–80
57. Li, X., Guan, Y., Li, Y., Wu, D., Liu, L., Deng, Q., *et al.* (2016) Effects of insulin-like growth factor-1 on the assembly and secretion of very low-density lipoproteins in cow hepatocytes in vitro. *Gen. Comp. Endocrinol.* **226**, 82–87
58. Ong, W-Y., Ng, M. P-E., Loke, S-Y., Jin, S., Wu, Y-J., Tanaka, K., *et al.* (2013) Comprehensive gene expression profiling reveals synergistic functional networks in cerebral vessels after hypertension or hypercholesterolemia. *PLoS One.* **8**, e68335
59. Shendre, A., Irvin, M. R., Wiener, H., Zhi, D., Limdi, N. A., Overton, E. T., *et al.* (2017) Local ancestry and clinical cardiovascular events among African Americans from the atherosclerosis risk in communities study. *J. Am. Heart Assoc.* **6**, e004739
60. Schroer, A. K., Bersi, M. R., Clark, C. R., Zhang, Q., Sanders, L. H., Hatzopoulos, A. K., *et al.* (2019) Cadherin-11 blockade reduces inflammation-driven fibrotic remodeling and improves outcomes after myocardial infarction. *JCI Insight.* **4**, e131545
61. Johnson, C. L., Riley, L., Bersi, M., Linton, M. F., and Merryman, W. D. (2021) Impaired macrophage trafficking and increased helper T-cell recruitment with loss of cadherin-11 in atherosclerotic immune response. *Am. J. Physiol. Heart Circ. Physiol.* **321**, H756–H769
62. Rainwater, D. L., VandeBerg, J. L., and Mahaney, M. C. (2010) Effects of diet on genetic regulation of lipoprotein metabolism in baboons. *Atherosclerosis.* **213**, 499–504
63. Nelson, M. E., Madsen, S., Cooke, K. C., Fritzen, A. M., Thorius, I. H., Masson, S. W. C., *et al.* (2022) Systems-level analysis of insulin action in mouse strains provides insight into tissue- and pathway-specific interactions that drive insulin resistance. *Cell Metab.* **34**, 227–239.e226
64. Yam, P., Albright, J., VerHague, M., Gertz, E. R., Pardo-Manuel de Villena, F., and Bennett, B. J. (2020) Genetic background shapes phenotypic response to diet for adiposity in the collaborative cross. *Front. Genet.* **11**, 615012
65. Field, B. C., Gordillo, R., and Scherer, P. E. (2020) The role of ceramides in diabetes and cardiovascular disease regulation of ceramides by adipokines. *Front. Endocrinol. (Lausanne).* **11**, 569250
66. Tippetts, T. S., Holland, W. L., and Summers, S. A. (2021) Cholesterol – the devil you know; ceramide – the devil you don't. *Trends Pharmacol. Sci.* **42**, 1082–1095
67. Akhiyat, N., Vasile, V., Ahmad, A., Sara, J. D., Nardi, V., Lerman, L. O., *et al.* (2022) Plasma ceramide levels are elevated in patients with early coronary atherosclerosis and endothelial dysfunction. *J. Am. Heart Assoc.* **11**, e022852
68. Wang, P., Zeng, G., Yan, Y., Zhang, S-Y., Dong, Y., Zhang, Y., *et al.* (2022) Disruption of adipocyte HIF-1α improves atherosclerosis through the inhibition of ceramide generation. *Acta Pharm. Sin. B.* **12**, 1899–1912
69. Chakraborty, M., Lou, C., Huan, C., Kuo, M-S., Park, T-S., Cao, G., *et al.* (2013) Myeloid cell–specific serine palmitoyltransferase subunit 2 haploinsufficiency reduces murine atherosclerosis. *J. Clin. Invest.* **123**, 1784–1797
70. Yu, Z., Peng, Q., Li, S., Hao, H., Deng, J., Meng, L., *et al.* (2020) Myriocin and d-PDMP ameliorate atherosclerosis in ApoE−/− mice via reducing lipid uptake and vascular inflammation. *Clin. Sci.* **134**, 439–458

71. Park, T-S., Rosebury, W., Kindt, E. K., Kowala, M. C., and Panek, R. L. (2008) Serine palmitoyltransferase inhibitor myriocin induces the regression of atherosclerotic plaques in hyperlipidemic ApoE-deficient mice. *Pharmacol. Res.* **58**, 45–51
72. Li, Z., Park, T-S., Li, Y., Pan, X., Iqbal, J., Lu, D., *et al.* (2009) Serine palmitoyltransferase (SPT) deficient mice absorb less cholesterol. *Biochim. Biophys. Acta Mol. Cell Biol. Lipids.* **1791**, 297–306
73. Hojjati, M. R., Li, Z., Zhou, H., Tang, S., Huan, C., Ooi, E., *et al.* (2005) Effect of myriocin on plasma sphingolipid metabolism and atherosclerosis in apoE-deficient mice. *J. Biol. Chem.* **280**, 10284–10289
74. Johnson, E. L., Heaver, S. L., Waters, J. L., Kim, B. I., Bretin, A., Goodman, A. L., *et al.* (2020) Sphingolipids produced by gut bacteria enter host metabolic pathways impacting ceramide levels. *Nat. Commun.* **11**, 2471
75. Gu, X., Sun, R., Chen, L., Chu, S., Doll, M. A., Li, X., *et al.* (2021) Neutral ceramidase mediates nonalcoholic steatohepatitis by regulating monounsaturated fatty acids and gut IgA(+) B cells. *Hepatology.* **73**, 901–919
76. Flowers, M. T., Groen, A. K., Oler, A. T., Keller, M. P., Choi, Y., Schueler, K. L., *et al.* (2006) Cholestasis and hypercholesterolemia in SCD1-deficient mice fed a low-fat, high-carbohydrate diets. *J. Lipid Res.* **47**, 2668–2680
77. Chu, K., Miyazaki, M., Man, W. C., and Ntambi, J. M. (2006) Stearoyl-coenzyme A desaturase 1 deficiency protects against hypertriglyceridemia and increases plasma high-density lipoprotein cholesterol induced by liver X receptor activation. *Mol. Cell. Biol.* **26**, 6786–6798
78. Vitali, C., Khetarpal, S. A., and Rader, D. J. (2017) HDL cholesterol metabolism and the risk of CHD: new insights from human genetics. *Curr. Cardiol. Rep.* **19**, 132
79. Brunham, L. R., Singaraja, R. R., Duong, M., Timmins, J. M., Fievet, C., Bissada, N., *et al.* (2009) Tissue-specific roles of ABCA1 influence susceptibility to atherosclerosis. *Arterioscler. Thromb. Vasc. Biol.* **29**, 548–554
80. Brunham, L. R., Singaraja, R. R., and Hayden, M. R. (2006) Variations on a gene: rare and common variants in ABCA1 and their impact on HDL cholesterol levels and atherosclerosis. *Annu. Rev. Nutr.* **26**, 105–129
81. Singaraja, R. R., Brunham, L. R., Visscher, H., Kastelein, J. J. P., and Hayden, M. R. (2003) Efflux and atherosclerosis. *Arterioscler. Thromb. Vasc. Biol.* **23**, 1322–1332
82. Hoekstra, M. (2017) SR-BI as target in atherosclerosis and cardiovascular disease - a comprehensive appraisal of the cellular functions of SR-BI in physiology and disease. *Atherosclerosis.* **258**, 153–161
83. Braun, A., Trigatti, B. L., Post, M. J., Sato, K., Simons, M., Edelberg, J. M., *et al.* (2002) Loss of SR-BI expression leads to the early onset of occlusive atherosclerotic coronary artery disease, spontaneous myocardial infarctions, severe cardiac dysfunction, and premature death in apolipoprotein E–deficient mice. *Circ. Res.* **90**, 270–276
84. Zanoni, P., Khetarpal, S. A., Larach, D. B., Hancock-Cerutti, W. F., Millar, J. S., Cuchel, M., *et al.* (2016) Rare variant in scavenger receptor BI raises HDL cholesterol and increases risk of coronary heart disease. *Science.* **351**, 1166–1171
85. Edsfeldt, A., Dunér, P., Ståhlman, M., Mollet, I. G., Asciutto, G., Grufman, H., *et al.* (2016) Sphingolipids contribute to human atherosclerotic plaque inflammation. *Arterioscler. Thromb. Vasc. Biol.* **36**, 1132–1140
86. Poss, A. M., Maschek, J. A., Cox, J. E., Hauner, B. J., Hopkins, P. N., Hunt, S. C., *et al.* (2020) Machine learning reveals serum sphingolipids as cholesterol-independent biomarkers of coronary artery disease. *J. Clin. Invest.* **130**, 1363–1376
87. Kurano, M., and Yatomi, Y. (2018) Sphingosine 1-phosphate and atherosclerosis. *J. Atheroscler. Thromb.* **25**, 16–26
88. Kim, M., Huda, M. N., Evans, L. W., Que, E., Gertz, E. R., Maeda-Smithies, N., *et al.* (2023) Integrative analysis of hepatic transcriptional profiles reveals genetic regulation of atherosclerosis in hyperlipidemic diversity outbred-F1 mice. *Sci. Rep.* **13**, 9475